analytical chemistry

pubs.acs.org/ac

Article

Conductive Covalent Organic Frameworks with Conductivity- and Pre-Reduction-Enhanced Electrochemiluminescence for Ultrasensitive Biosensor Construction

Jin-Ling Zhang, Li-Ying Yao, Yang Yang, Wen-Bin Liang, Ruo Yuan, and Dong-Rong Xiao*

Cite This: *Anal. Chem.* 2022, 94, 3685−3692

Read Online

ACCESS | Metrics & More | Article Recommendations | Supporting Information

ABSTRACT: Covalent organic frameworks (COFs) have attracted widespread attention in the electrochemiluminescence (ECL) field owing to their high load capacity of ECL luminophores and porous structures, but their ECL performance is still limited by the intrinsic poor conductivity (generally $<10^{-8}$ S m^{-1}). To address this shortcoming, we used 2,3,6,7,10,11-hexaaminotriphenylene (HATP) and 2,3,6,7,10,11-hexahydroxytriphenylene (HHTP) to synthesize a conductive COF (HHTP-HATP-COF, conductivity = 3.11×10^{-4} S m^{-1}). Compared with HATP, HHTP, and low-conductive HHTP-DABZ-COF, HHTP-HATP-COF exhibited superior ECL performance, not only because HHTP-HATP-COF possessed massive ECL luminophores but also because its conductive porous framework accelerated charge transport in the whole framework and improved the utilization ratio of ECL luminophores. More interestingly, the ECL intensity of the HHTP-HATP-COF/$S_2O_8^{2-}$ system was further improved after pre-reduction electrolysis due to the accumulation of HHTP-HATP-COF cation radicals. The experimental results showed that the ECL intensity of the HHTP-HATP-COF/$S_2O_8^{2-}$ system after pre-reduction was about 1.64-, 3.96-, 6.88-, and 8.09-fold higher than those of HHTP-HATP-COF/$S_2O_8^{2-}$, HHTP-DABZ-COF/$S_2O_8^{2-}$, HHTP/$S_2O_8^{2-}$, and HATP/$S_2O_8^{2-}$ systems, respectively. Considering the superior ECL property of the HHTP-HATP-COF/$S_2O_8^{2-}$ system after pre-reduction, it was used as a high-efficient ECL beacon together with an aptamer/protein proximity binding-induced three-dimensional bipedal DNA walker to construct an ultrasensitive biosensor for thrombin detection, which displayed broad linearity (100 aM to 1 nM) with a detection limit of 62.1 aM. Overall, the work offered effective ways to increase ECL performance by the enhancement of conductivity and by the pre-reduction, proposing new ideas to design high-efficiency COF-based ECL materials and endowing conductive COFs with ECL biosensor application for the first time.

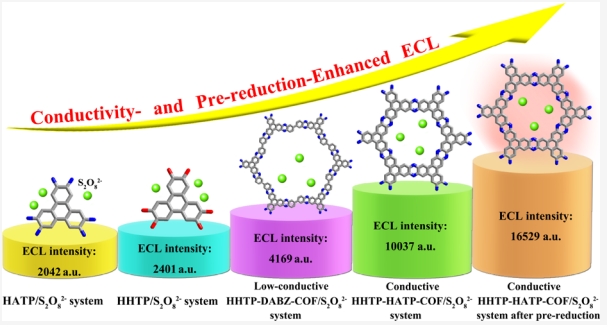

INTRODUCTION

Electrochemiluminescence (ECL) is the phenomenon in which the electrochemically generated radicals undergo electron-transfer reactions on the electrode surface to produce excited states, and then, the excited states return to the ground state and simultaneously emit light.[1−3] Benefitting from its outstanding controllability, high sensitivity, inexpensive cost, and low-background noise, ECL technology has been extensively used in the clinical detection of proteins, nucleic acids, small molecules, *etc.*[4−6] With the increasing requirements for detection sensitivity of trace biomolecules in clinical analysis, it is very necessary to develop highly efficient ECL emitters with strong initial ECL intensities to construct high-sensitivity ECL sensors.[7−9] In recent years, to enhance the ECL intensity, different types of materials, including silica nanoparticles (NPs),[10] carbon nanotubes (CNTs),[11] metal−organic frameworks (MOFs),[12] metal−organic layers (MOLs),[13] and covalent organic frameworks (COFs),[14] have been employed as carriers to load ECL luminophores. Among them, COFs, as a burgeoning type of porous crystalline material, have aroused great research interest in the ECL field recently because their high porosity and very large surface areas not only could significantly heighten the immobilization amount of ECL luminophores but also facilitated the excitation of external and internal ECL luminophores to realize strong ECL emission.[15−19] Very recently, Luo and co-workers used the aggregation-induced emission (AIE)-active 4,4′-dia-mino-2,2′-bipyridine to synthesize an ECL-active COF with nanozyme Co_3O_4 as an amplification element.[20] Our group found that the COF nanosheet formed by covalent connections between pyrene luminophores and cyano-substituted phenylenevinylenes (AIE luminogens) possessed stronger ECL emission and higher ECL efficiency than those of

Received: December 15, 2021
Accepted: February 4, 2022
Published: February 14, 2022

Downloaded via TSINGHUA UNIV on November 4, 2022 at 01:58:08 (UTC).
See https://pubs.acs.org/sharingguidelines for options on how to legitimately share published articles.

ACS Publications

© 2022 American Chemical Society

https://doi.org/10.1021/acs.analchem.1c05436
Anal. Chem. 2022, 94, 3685−3692

its monomer.[14] Although the ECL intensities and efficiencies of the ECL-active COFs have been improved to a certain extent, the utilization ratio of the ECL luminophores is still limited by the poor intrinsic electronic conductivity of COFs (generally $<10^{-8}$ S m^{-1}).[21] Hence, it is highly desirable to rationally design and construct novel COFs combining the high loading capacity of ECL luminophores with high electronic conductivity.

The two-dimensional (2D) conductive COFs with transversely extended π-conjugated structures not only inherit the merits of COFs with low density, high specific surface area, tunable porosity, robust thermal, and chemical stability but also possess excellent electrical conductivity.[21−24] In recent years, increasing research efforts have been devoted to the design and synthesis of 2D conductive COFs. In 2014, Jiang *et al.* synthesized a 2D p-type imine-linked conductive COF by using 2,3,6,7-tetra(4-formylphenyl) tetrathiafulvalene and 1,4-phenyldiamine as monomers.[25] After that, Dincă and Duhović prepared a series of boronic ester-based 2D conductive COFs by condensation of benzodichalcogenophene diboronic acids with 2,3,6,7,10,11-hexahydroxytriphenylene (HHTP).[26] Very recently, Li and co-workers prepared a 2D conductive COF connected by C−C single bonds through the self-polymerization of tetrakis(4-thiophenephenyl)porphyrin monomers for lithium storage.[27] However, the conductivity of the 2D conductive COFs was still hindered by the weak charge transfer capability of linking units between aromatic moieties. In addition, till now, most studies on conductive COFs have centered on the optimization of electric conductivity, pore size, and surface area, whereas conductive COFs with strong ECL emission have not been reported. Thus, it is necessary and significant to design and synthesize fully π-conjugated 2D COFs combined with high electronic conductivity and strong ECL emission.

In 2019, Feng's group reported that using pyrazine units as linkages could improve the charge transport capacity of 2D COFs by increasing the π-conjugation of the framework.[28] Furthermore, HHTP and 2,3,6,7,10,11-hexaaminotriphenylene (HATP) with a large π-conjugated planar structure have been extensively used as organic ligands to synthesize conductive MOFs.[29−31] Inspired by the aforementioned studies, we surmised that high-conductive COFs can be obtained by connecting HHTP and HATP *via* pyrazine linkages. With this in mind, we used HHTP and HATP in the aid of 2,3-dichloro-5,6-dicyano-1,4-benzoquinone (DDQ) and trifluoroacetic acid (TFA) to synthesize a fully π-conjugated pyrazine-linked conductive COF (HHTP-HATP-COF) with a highly planar structure (Scheme 1A). As expected, the obtained HHTP-HATP-COF exhibited superior electronic conductivity (3.11×10^{-4} S m^{-1}) and splendid ECL emission. The possible reasons for the strong ECL emission could be attributed to the following three points. (i) The superior electronic conductivity of the HHTP-HATP-COF was beneficial to the electron transfer in the whole structure, which made more ECL luminophores susceptible to be electrochemically activated, thus resulting in a strong ECL emission. (ii) The HHTP luminophore and the HATP luminophore were directly used as organic monomers to synthesize the conductive HHTP-HATP-COF (Scheme 1A and Figure S1A), which could significantly enhance the immobilization amount of the ECL luminophores, thus leading to an enhanced ECL emission. (iii) The porous framework of HHTP-HATP-COF allowed the electrolyte containing the co-reactant ($S_2O_8^{2-}$) to diffuse into

Scheme 1. (A) Synthesis of HHTP-HATP-COF. (B) Process of the Aptamer/Protein Proximity Binding-Induced 3D Bipedal DNA Walker Amplification. (C) Preparation Procedures of the Proposed ECL Sensor

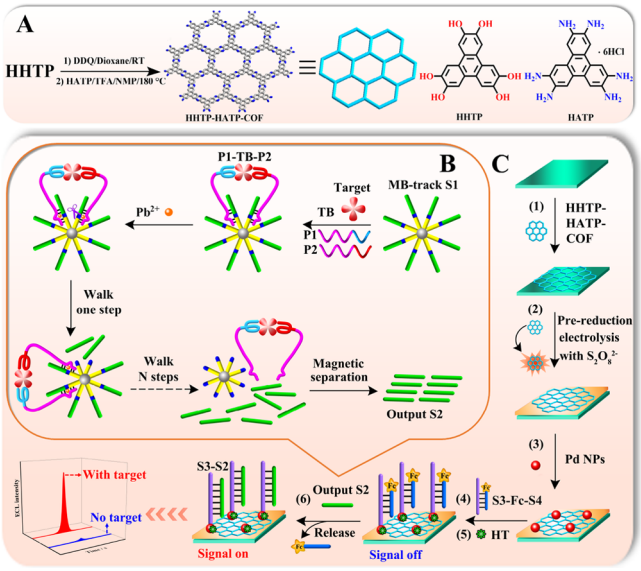

the internal of the framework, which was conducive to the electrochemical activation of the internal ECL luminophores and increased their utilization ratio, thereby realizing the further improvement of the ECL signal. More interestingly, the ECL intensity of the HHTP-HATP-COF/$S_2O_8^{2-}$ system was further remarkably improved after pre-reduction electrolysis on the electrode.[32,33] As expected, the experimental results revealed that the average ECL intensity of the HHTP-HATP-COF/$S_2O_8^{2-}$ system after pre-reduction electrolysis was about 1.64, 3.96, 6.88, and 8.09 times higher than those of HHTP-HATP-COF/$S_2O_8^{2-}$, low-conductive HHTP-DABZ-COF/$S_2O_8^{2-}$ (Figure S1B), HHTP/$S_2O_8^{2-}$, and HATP/$S_2O_8^{2-}$ systems under identical conditions, respectively. Furthermore, compared with the HHTP-HATP-COF/$S_2O_8^{2-}$, low-conductive HHTP-DABZ-COF/$S_2O_8^{2-}$, HHTP/$S_2O_8^{2-}$, and HATP/$S_2O_8^{2-}$ systems, the ECL efficiency of the HHTP-HATP-COF/$S_2O_8^{2-}$ system after pre-reduction electrolysis was also greatly improved. Additionally, it is impressive that, after HHTP-HATP-COF was soaked in water at room temperature for 3 months, the ECL intensities of the HHTP-HATP-COF/$S_2O_8^{2-}$ system with and without pre-reduction almost remained unchanged due to the outstanding water stability of HHTP-HATP-COF.

Thrombin (TB) is regarded as an important biomarker associated with many diseases such as cardiovascular diseases, thromboembolic disease, and inflammation reactions.[34−36] At present, many analysis methods, such as ECL,[34] fluorescence,[35] photoelectrochemistry,[36] and electrochemistry,[37] have been used for the detection of TB. Among them, ECL has drawn great attention owing to its low detection limit, wide detection range, and excellent stability.[34] Considering the advantages of the ECL method and the excellent ECL performance of the HHTP-HATP-COF/$S_2O_8^{2-}$ system after pre-reduction, we used the HHTP-HATP-COF/$S_2O_8^{2-}$ system after pre-reduction electrolysis as a high-efficient ECL signal tag combined with the aptamer/protein proximity binding-induced 3D bipedal DNA walker to construct an "off−on" ECL sensor for ultrasensitive TB detection. As displayed in

https://doi.org/10.1021/acs.analchem.1c05436
Anal. Chem. 2022, 94, 3685−3692

Scheme 1C, initially, the prepared HHTP-HATP-COF was dropped onto the surface of a bare glassy carbon electrode (GCE) to form a homogeneous film. After pre-reduction electrolysis of the HHTP-HATP-COF on the GCE with $S_2O_8^{2-}$, a strong initial ECL signal was attained. Then, the palladium NPs (Pd NPs) were anchored on the above-modified electrode to form a Pd NP film for subsequent DNA immobilization. After that, the double-stranded DNA (S3-Fc-S4) formed by the hybridization of thiol-labeled single-stranded DNA3 (ssDNA3, S3) and ferrocene-labeled ssDNA4 (Fc-S4) was immobilized on the above-modified electrode *via* the Pd−S bond to quench the ECL (signal off). Meanwhile, with the aid of the signal amplification strategy of the aptamer/protein proximity binding-induced 3D bipedal DNA walker, a small amount of target TB was transformed into numerous output S2 (Scheme 1B). Concretely, after the target TB was introduced, a pair of proximity probes (P1 and P2) was simultaneously bound with one TB *via* the TB aptamer to form a P1-TB-P2 complex, which brought the tail sequences (the "feet") of probes into close proximity and drove the "feet" of probes to hybridize with the tracks S1 to produce the recognition sites for Pb^{2+}. After the introduction of Pb^{2+}, the tracks S1 were cut into two parts, resulting in the release of S2 from the magnetic bead surface. Meanwhile, the P1-TB-P2 complex walked on the broad 3D track and repeated the above procedures to achieve the high-efficiency cleavage of track S1, producing massive output S2. When output S2 was added to the electrode surface, it was captured by the S3 to make massive Fc-S4 be removed from the surface of the electrode surface. Thus, the ECL signal of the sensor recovered to a "signal-on" state. As expected, the constructed ECL sensor realized the supersensitive detection of target TB. Meaningfully, the conductivity- and pre-reduction-enhanced ECL based on COFs provided promising and efficient approaches for improving ECL intensity and efficiency, which opened a new page for the development of high-efficient ECL materials and thus broadened the applied range of conductive COFs.

EXPERIMENTAL SECTION

The Preparation of HHTP-HATP-COF. First, 12.0 mg of HHTP (0.036 mmol), 8.2 mg of DDQ (0.036 mmol), and 0.6 mL of 1,4-dioxane were mixed in a vial and stirred at room temperature for 24 h. After the reaction was completed, the mixture was centrifuged to collect the intermediate product. Subsequently, the obtained intermediate product, 16.5 mg of HATP (0.03 mmol), 10 mL of *N*-methyl-2-pyrrolidone, and 2.5 μL of trifluoroacetic acid were mixed in a pressure tube. After the above mixture was sonicated for 10 min, it was heated in an oven at 180 °C for 2 days. The obtained mixture was naturally cooled to room temperature and subsequently dialyzed with *N*-methyl-2-pyrrolidone to remove the redundant materials and oligomers. Furthermore, the *N*-methyl-2-pyrrolidone was replaced every day. The obtained suspension was precipitated with ether, collected by centrifugation, washed several times with methanol, and finally dried under vacuum to obtain HHTP-HATP-COF.

The ECL Sensor Preparation Procedure. First, each glassy carbon electrode (GCE) was polished with an alumina slurry and rinsed with deionized water to obtain a glossy and clean surface. Next, the GCE was modified with 12 μL dispersion of HHTP-HATP-COF (1 mg/mL) to gain the HHTP-HATP-COF/GCE. Then, the HHTP-HATP-COF/GCE was anchored with 7 μL of Pd NPs to obtain the Pd NPs/HHTP-HATP-COF/GCE. After that, the prepared S3-Fc-S4 (10 μL) was incubated on the above-prepared electrode surface at 4 °C for 12 h. Following that, 10 μL of hexanethiol was incubated on the S3-Fc-S4/Pd NPs/HHTP-HATP-COF/GCE for 90 min to eliminate the nonspecific binding effect. Finally, the HT/S3-Fc-S4/Pd NPs/HHTP-HATP-COF/GCE was incubated with 10 μL of output S2 at 37 °C for 2 h to achieve a strand displacement reaction. It is worth pointing out that the electrode ought to be washed with deionized water after each step of incubation.

ECL Detection of the Proposed Sensor. After the above-modified GCEs were pre-reduced, they were placed in a 2 mL phosphate-buffered solution (PBS) containing 0.01 M $S_2O_8^{2-}$ with a scanning potential of −2 to 0 V for ECL detection.

RESULTS AND DISCUSSION

Characterization of HHTP-HATP-COF. To verify the successful synthesis of HHTP-HATP-COF, its crystallinity was investigated by powder X-ray diffraction (PXRD). As displayed in Figure S2, the peaks of HHTP-HATP-COF were in agreement with the peaks of the simulated XRD pattern. To further validate the formation of HHTP-HATP-COF, it was characterized by Fourier transform infrared (FT-IR) spectroscopy. As presented in Figure S3, the N−H stretching vibration band at 3336 cm^{-1} belonged to the amino group of the HATP monomer and the O−H stretching band at 3407 cm^{-1} pertained to the hydroxyl group of the HHTP monomer that was obviously attenuated after the reaction, while the characteristic C═N stretching bands at 1515, 1415, and 1396 cm^{-1} appeared,[38−40] demonstrating the formation of π-conjugated pyrazine linkages in the HHTP-HATP-COF framework. Furthermore, compared with the starting monomers, the UV−vis absorption spectrum of HHTP-HATP-COF showed a wider absorption, and the absorption onset had an obvious red shift, indicating the presence of a large π-conjugated system in the structure (Figure S4). The morphology of HHTP-HATP-COF was characterized by scanning electron microscopy (SEM) and transmission electron microscopy (TEM). As observed in Figure 1A,B and Figure S5, HHTP-HATP-COF displayed ultrathin sheet morphology. Moreover, the thickness of HHTP-HATP-COF measured by atomic force microscopy (AFM) was 5.64 ± 0.2 nm (Figure 1C,D), which corresponded to the thickness of few-layer HHTP-HATP-COF nanosheets. All the above experimental results indicated that the HHTP-HATP-COF was successfully synthesized.

Probable ECL Mechanism of the HHTP-HATP-COF/$S_2O_8^{2-}$ System and the Self-Enhanced Mechanism of the HHTP-HATP-COF/$S_2O_8^{2-}$ System after Pre-Reduction Electrolysis. To study the ECL behaviors of HHTP-HATP-COF in the cathodic system, cyclic voltammetry (CV), differential pulse voltammetry (DPV), and ECL responses were measured. As displayed in Figure 2A, a strong reduction peak was observed at approximately −1.3 V when the HHTP-HATP-COF-modified GCE was tested in PBS containing $S_2O_8^{2-}$ (curve c), indicating that $S_2O_8^{2-}$ was electro-reduced to a strongly oxidizing intermediate $SO_4^{\bullet-}$ ($E^\circ \geq 3.15$ V vs SCE) on the HHTP-HATP-COF/GCE (eq 1) and subsequently injected a hole into the highest occupied molecular orbital of HHTP-HATP-COF to form HHTP-HATP-COF$^{\bullet+}$ (eq 2).[33,41,42] Even though the reduction potential of $S_2O_8^{2-}$ on HHTP-HATP-COF/GCE was deferred compared with that of

https://doi.org/10.1021/acs.analchem.1c05436
Anal. Chem. 2022, 94, 3685−3692

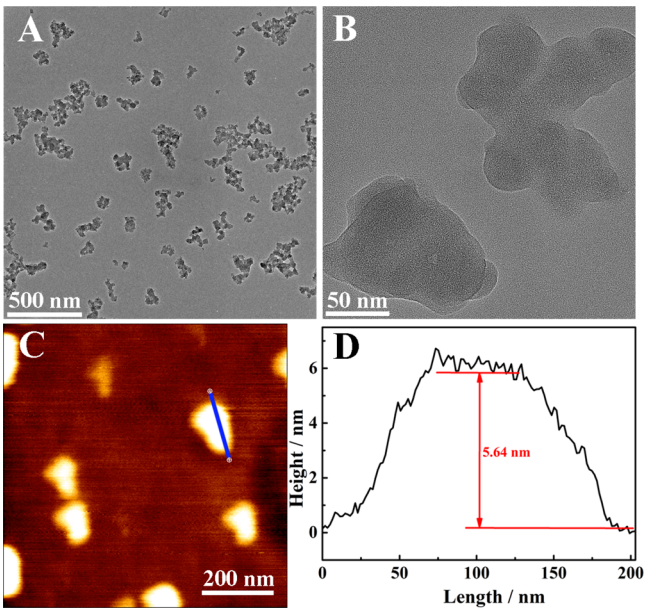

Figure 1. (A, B) TEM images of HHTP-HATP-COF. (C, D) AFM image and height profile of HHTP-HATP-COF.

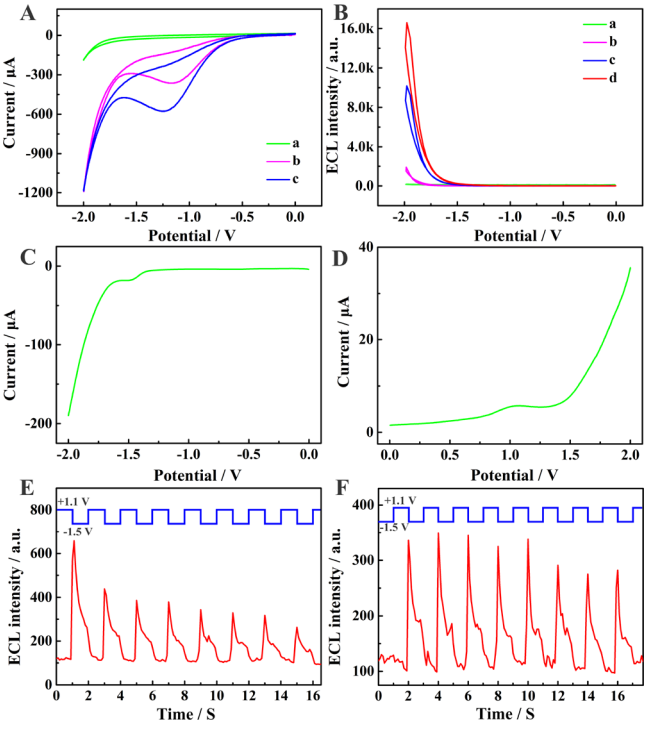

Figure 2. (A) CV curves of (a) HHTP-HATP-COF/GCE, (b) bare GCE, and (c) HHTP-HATP-COF/GCE in N_2-saturated PBS (a) without and (b, c) with 0.01 M $K_2S_2O_8$. (B) ECL intensities of (a) HHTP-HATP-COF/GCE, (b) bare GCE, and (c) HHTP-HATP-COF/GCE in N_2-saturated PBS (a) without and (b, c) with 0.01 M $K_2S_2O_8$; (d) HHTP-HATP-COF/GCE after pre-reduction electrolysis at −2 V for 3 min in N_2-saturated PBS containing 0.01 M $K_2S_2O_8$. (C) Cathodic and (D) anodic DPV of HHTP-HATP-COF/GCE in N_2-saturated PBS solution. Annihilation ECL of HHTP-HATP-COF/GCE in N_2-saturated PBS solution by stepping the potential (E) from +1.1 to −1.5 V and (F) from −1.5 to +1.1 V (PMT = 800 V).

$S_2O_8^{2-}$ on GCE (−1.1 V; Figure 2A, curve b), the oxidation of HHTP-HATP-COF with $SO_4^{\bullet-}$ (eq 2) obviously occurred earlier than the electrochemical reduction of HHTP-HATP-COF (eq 3) because HHTP-HATP-COF/GCE in PBS containing $S_2O_8^{2-}$ exhibited a more positive reduction potential (−1.3 V) than that in blank PBS solution (−1.5 V; Figure 2C).[41,42] Then, the HHTP-HATP-COF$^{\bullet-}$ reacted with HHTP-HATP-COF$^{\bullet+}$ and $SO_4^{\bullet-}$ to generate the excited-state HHTP-HATP-COF* (eqs 4 and 5), thereby yielding a strong ECL emission (Figure 2B, curve c).[2,43,44]

$$S_2O_8^{2-} + e^- \rightarrow SO_4^{2-} + SO_4^{\bullet-} \quad (1)$$

$$\text{HHTP} - \text{HATP} - \text{COF} + SO_4^{\bullet-} \rightarrow \text{HHTP} - \text{HATP} - \text{COF}^{\bullet+} + SO_4^{2-} \quad (2)$$

$$\text{HHTP} - \text{HATP} - \text{COF} + e^- \rightarrow \text{HHTP} - \text{HATP} - \text{COF}^{\bullet-} \quad (3)$$

$$\text{HHTP} - \text{HATP} - \text{COF}^{\bullet-} + \text{HHTP} - \text{HATP} - \text{COF}^{\bullet+} \rightarrow \text{HHTP} - \text{HATP} - \text{COF}^* + \text{HHTP} - \text{HATP} - \text{COF} \quad (4)$$

$$\text{HHTP} - \text{HATP} - \text{COF}^{\bullet-} + SO_4^{\bullet-} \rightarrow \text{HHTP} - \text{HATP} - \text{COF}^* + SO_4^{2-} \quad (5)$$

$$\text{HHTP} - \text{HATP} - \text{COF}^* \rightarrow \text{HHTP} - \text{HATP} - \text{COF} + h\nu \quad (6)$$

During the continuous ECL scanning, we found that the ECL signal of HHTP-HATP-COF increased continuously at the beginning of the test (Figure S7). According to the literature[33] and the ECL mechanism of HHTP-HATP-COF, we preliminarily speculated that the enhanced ECL signal was attributed to the accumulation of HHTP-HATP-COF cation radicals. To verify our speculation, the annihilation ECL of HHTP-HATP-COF was studied by the stepping pulse approach. As shown in Figure 2C,D, a reduction peak (−1.5 V) and an oxidation peak (+1.1 V) were observed when the HHTP-HATP-COF-modified GCE was measured in N_2-saturated PBS, which indicated that HHTP-HATP-COF possessed both oxidation and reduction properties. As displayed in Figure 2E, no ECL emission was observed by directly holding the HHTP-HATP-COF at an initial stepping potential of +1.1 V. Subsequently, an obvious ECL signal was gained when the second stepping potential stepped to −1.5 V because HHTP-HATP-COF was electro-reduced to HHTP-HATP-COF$^{\bullet-}$ at −1.5 V and then reacted with HHTP-HATP-COF$^{\bullet+}$ produced in the initial step to generate the excited-state HHTP-HATP-COF* for ECL emission. Figure 2F shows the ECL transients of HHTP-HATP-COF initiated by the reduction stepping potential. With an initial stepping potential of −1.5 V, which subsequently stepped to +1.1 V, almost no apparent ECL was observed in the first pulse cycle because the HHTP-HATP-COF$^{\bullet-}$ is not stable, thereby leading to the absence of radiative charge transfer. After that, when the stepping potential was changed from +1.1 to −1.5 V, an obvious ECL was observed. The experimental result revealed that the HHTP-HATP-COF$^{\bullet+}$ generated in the first pulse cycle indeed could be stable long enough in PBS solution to combine with the HHTP-HATP-COF$^{\bullet-}$ produced in the following step for annihilation ECL.

https://doi.org/10.1021/acs.analchem.1c05436
Anal. Chem. 2022, 94, 3685−3692

In addition, the ECL transients of HHTP-HATP-COF with the co-reactant were also investigated by stepping pulse to further verify our conjecture. As shown in Figure S8A, the cathodic ECL signal of HHTP-HATP-COF progressively strengthened, which further indicated that the ECL enhancement was caused by the cumulation of HHTP-HATP-COF$^{\bullet+}$ in the course of stepping pulse. On the contrary, the anodic ECL signal of HHTP-HATP-COF gradually decreased (Figure S8B), which was caused by the consumption of the HHTP-HATP-COF$^{\bullet+}$ by the triethylamine radical (the anodic ECL behaviors of the HHTP-HATP-COF are shown in the Supporting Information, Section S12). This indirectly proved that the ECL signal of HHTP-HATP-COF could increase with the cumulation of HHTP-HATP-COF$^{\bullet+}$.

Based on the aforementioned test results, we speculated that the HHTP-HATP-COF$^{\bullet+}$ radicals could be deliberately accumulated through pre-reduction electrolysis, thereby enhancing the ECL signal of the HHTP-HATP-COF/$S_2O_8^{2-}$ system. Therefore, pre-reduction electrolysis was used to preprocess the HHTP-HATP-COF/$S_2O_8^{2-}$ system for gaining a stronger ECL signal. To acquire the optimal ECL signal, the potential of pre-reduction electrolysis and the time of pre-reduction electrolysis were optimized (see details in the Supporting Information, Section S13). Under the optimum test conditions, the ECL intensity of the HHTP-HATP-COF/$S_2O_8^{2-}$ system after pre-reduction treatment was increased to 16,529 a.u. (Figure 2B, curve d), which was about 1.64-fold higher than that of the HHTP-HATP-COF/$S_2O_8^{2-}$ system (10,037 a.u; Figure 2B, curve c). These results demonstrated that the pre-reduction electrolysis was an effectual method for enhancing the ECL signal.

According to the above-mentioned experimental results, the self-enhanced mechanism of the HHTP-HATP-COF/$S_2O_8^{2-}$ system after pre-reduction electrolysis is depicted in Figure 3.

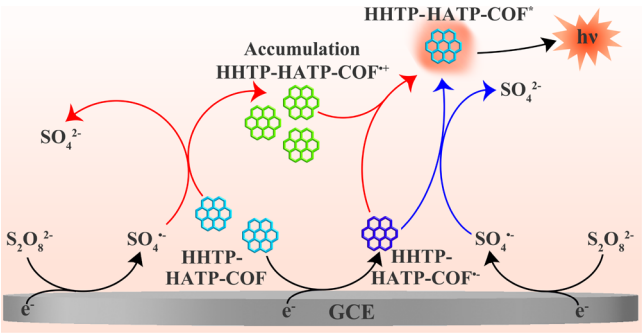

Figure 3. Self-enhanced ECL mechanism of the HHTP-HATP-COF/$S_2O_8^{2-}$ system after pre-reduction electrolysis.

Under the pre-reduction conditions, $S_2O_8^{2-}$ was electrochemically reduced to $SO_4^{\bullet-}$ and then reacted with HHTP-HATP-COF to produce a large number of HHTP-HATP-COF$^{\bullet+}$.[33] Once HHTP-HATP-COF was electrochemically reduced to HHTP-HATP-COF$^{\bullet-}$, HHTP-HATP-COF$^{\bullet-}$ reacted with the accumulated HHTP-HATP-COF$^{\bullet+}$ as well as $SO_4^{\bullet-}$ to form the excited state of HHTP-HATP-COF*, resulting in a strong ECL emission.

Study of the ECL Performance. To study the effect of porosity on the ECL intensity, the ECL intensities of the porous HHTP-DABZ-COF (Figure S1B), nonporous HHTP (Scheme 1A), and nonporous HATP (Scheme 1A) were tested in PBS solution containing $S_2O_8^{2-}$. As seen in Figure 4A, the

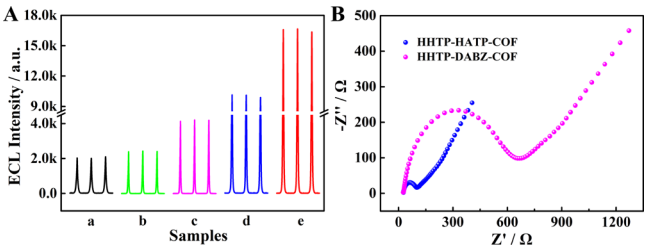

Figure 4. (A) ECL intensities of (a) HATP/$S_2O_8^{2-}$ system, (b) HHTP/$S_2O_8^{2-}$ system, (c) HHTP-DABZ-COF/$S_2O_8^{2-}$ system, (d) HHTP-HATP-COF/$S_2O_8^{2-}$ system, and (e) HHTP-HATP-COF/$S_2O_8^{2-}$ system after pre-reduction electrolysis. (B) Nyquist plots of the HHTP-DABZ-COF and HHTP-HATP-COF. The Nyquist plots were tested in 0.1 M PBS containing 5.0 mM $[Fe(CN)_6]^{3-/4-}$ and 0.1 M KCl with an excitation signal of 5 mV, formal potential of 220 mV, and frequency of 1.0×10^{-1} to 1.0×10^{5} Hz.

ECL intensity of the HHTP-DABZ-COF/$S_2O_8^{2-}$ system was 4169 a.u. (curve c), which was stronger than those of the HHTP/$S_2O_8^{2-}$ system (2401 a.u., curve b;) and HATP/$S_2O_8^{2-}$ system (2042 a.u., curve a). The reason might be that the porous structure of HHTP-DABZ-COF enabled the co-reactants to diffuse into the interior of the framework, which made more ECL luminophores to be excited, thus resulting in an increase in the ECL signal.

To confirm the validity of the conductivity-enhanced ECL effect, the electrical conductivities of HHTP-HATP-COF and HHTP-DABZ-COF were studied. The electrical conductivities of HHTP-HATP-COF and HHTP-DABZ-COF at room temperature were 3.11×10^{-4} and 2.98×10^{-5} S m^{-1}, respectively. This result indicated that HHTP-HATP-COF has better conductivity than HHTP-DABZ-COF. To further prove the above conclusion, the Nyquist plots of different modified electrodes were measured. From Figure 4B, we found that the HHTP-HATP-COF-modified electrode exhibited a much smaller semicircle than the HHTP-DABZ-COF-modified electrode, which indicated that HHTP-HATP-COF had lower electron-transfer resistance and higher electrical conductivity. Meanwhile, the ECL intensities of the conductive HHTP-HATP-COF/$S_2O_8^{2-}$ system and low-conductive HHTP-DABZ-COF/$S_2O_8^{2-}$ system were also tested and compared. As seen in Figure 4A, the ECL signal of the HHTP-HATP-COF/$S_2O_8^{2-}$ system (10,037 a.u, curve d) was much higher than that of the HHTP-DABZ-COF/$S_2O_8^{2-}$ system (4169 a.u., curve c) because the outstanding electrical conductivity of HHTP-HATP-COF could promote charge transport and make more ECL luminophores susceptible to be electrochemically activated. These experimental results indicated that enhancing the conductivity of ECL emitters can significantly increase their ECL intensity. More interestingly, the ECL intensity of the HHTP-HATP-COF/$S_2O_8^{2-}$ system was enhanced to 16,529 a.u. (Figure 4A, curve e) after on-electrode pre-reduction electrolysis, which was about 1.64-, 3.96-, 6.88-, and 8.09-fold higher than those of HHTP-HATP-COF/$S_2O_8^{2-}$, low-conductive HHTP-DABZ-COF/$S_2O_8^{2-}$, HHTP/$S_2O_8^{2-}$, and HATP/$S_2O_8^{2-}$ systems, respectively.[32,33] In addition, it was surprising that, after soaking HHTP-HATP-COF in water for 3 months at room temperature, the ECL intensities of the HHTP-HATP-COF/$S_2O_8^{2-}$ system and HHTP-HATP-COF/$S_2O_8^{2-}$ system after pre-reduction electrolysis almost remained unchanged owing to the splendid water stability of HHTP-HATP-COF (Figure S10A,B).

https://doi.org/10.1021/acs.analchem.1c05436
Anal. Chem. 2022, 94, 3685−3692

ECL efficiency is another key indicator to evaluate ECL performance of the ECL material. To fully understand the effect of the electrical conductivity and pre-reduction electrolysis on the ECL performance of the ECL materials, the ECL efficiencies of the HHTP-HATP-COF/$S_2O_8^{2-}$ system after pre-reduction electrolysis, HHTP-HATP-COF/$S_2O_8^{2-}$ system, HHTP-DABZ-COF/$S_2O_8^{2-}$ system, HHTP/$S_2O_8^{2-}$ system, and HATP/$S_2O_8^{2-}$ system are measured and compared (the calculation method is shown in Section S17 of the Supporting Information). As presented in Table S2, the ECL efficiency of the HHTP-HATP-COF/$S_2O_8^{2-}$ system after pre-reduction electrolysis was about 1.82, 2.51, 5.44, and 5.27 times those of HHTP-HATP-COF/$S_2O_8^{2-}$, HHTP-DABZ-COF/$S_2O_8^{2-}$, HHTP/$S_2O_8^{2-}$, and HATP/$S_2O_8^{2-}$ systems, respectively. These test results verified that the porous conductive HHTP-HATP-COF could be used as an outstanding ECL material, and the pre-reduction electrolysis was an effective strategy for improving ECL intensity and efficiency of the HHTP-HATP-COF/$S_2O_8^{2-}$ system.

Sensitivity of the Designed ECL Sensor. To appraise the sensitivity of the designed ECL sensor, the ECL responses of the designed sensor to a variety of concentrations of TB were measured under the optimum experimental conditions. As presented in Figure 5A, the ECL response of the sensor

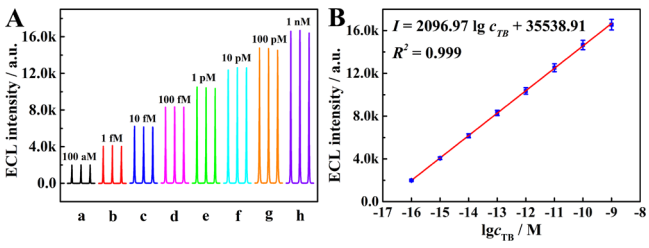

Figure 5. (A) ECL signals of the constructed sensor with different concentrations of TB. (B) Linear relationship of ECL intensity versus the logarithm of the TB concentration.

enhanced gradually with the increment of the TB concentration in the scope of 100 aM to 1 nM. As illustrated in Figure 5B, the ECL intensity (I) of the sensor was proportional to the logarithm of the TB concentration ($\lg c_{TB}$) and the regression equation could be expressed as I = 2096.97$\lg c_{TB}$ + 35,538.91 (the correlation coefficient is 0.999). The limit of detection was determined to be 62.1 aM based on the 3σ calculation. Furthermore, compared with the previously reported TB detection method (Table 1), our ECL biosensor exhibited a higher detection sensitivity, indicating that the sensor had a bright application prospect.

Stability, Specificity, and Reproducibility of the ECL Sensor. The stability, specificity, and reproducibility were the vital indicators to evaluate the performance of the ECL sensor. Hence, the stability of the designed sensor was studied by monitoring its response to different concentrations of TB (100 and 1 pM) under successive 22 cyclic scans. As presented in Figure 6A,B, the ECL signals concurrently exhibited

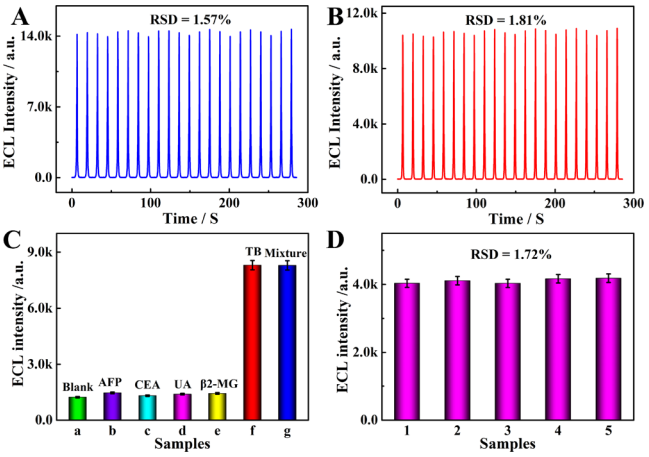

Figure 6. Stability of the ECL sensor with (A) 100 pM TB and (B) 1 pM TB. (C) Selectivity of the designed sensor with target TB and various interfering substances: (a) blank sample, (b) 10 pM AFP, (c) 10 pM CEA, (d) 10 pM UA, (e) 10 pM β2-MG, (f) 100 fM target TB, and (g) the mixture (10 pM AFP, 10 pM CEA, 10 pM UA, 10 pM β2-MG, and 100 fM target TB). (D) Reproducibility of the designed sensor incubated with 1 fM TB.

inappreciable fluctuation, and the relative standard deviations (RSDs) were 1.57% (100 pM) and 1.46% (1 pM) separately. It showed that the TB sensor possessed wonderful stability.

Meanwhile, to validate the specificity of the TB sensor, four different biomolecules, including α-1-fetoprotein (AFP), carcinoembryonic antigen (CEA), uric acid (UA), and β2-microglobulin (β2-MG), were employed as interferences. As seen in Figure 6C, the target TB (100 fM) caused a remarkable signal enhancement compared with the blank sample, while the AFP, CEA, UA, and β2-MG even at 100-fold concentration (10 pM) still caused no apparent signal change. In addition, the ECL response of the designed sensor incubated with the mixture solution (10 pM AFP, 10 pM CEA, 10 pM UA, 10 pM β2-MG, and 100 fM target TB) was almost the same as that of the target TB sample (100 fM). These results fully proved that the designed sensor had high specificity for target TB. Furthermore, five parallel sensors incubated with 1 fM TB were employed to study the reproducibility (Figure 6D), which all exhibited nearly equal ECL response with an RSD of 1.72%, confirming superior reproducibility of the constructed sensor.

Application. To estimate the feasibility of the designed sensor in practical samples, different concentrations of TB spiked into 10-fold diluted human serum were chosen to accomplish the recovery tests. As presented in Table 2, the

Table 1. Comparison of TB Detection Based on Various Methods

detection methods	linear range	detection limit	ref
fluorescence	5−120 nM	3.3 nM	35
photoelectrochemistry	10 fM to 1 μM	1.41 fM	36
electrochemistry	1 fM to 10 nM	0.3 fM	37
ECL	10 fM to 1 nM	1.82 fM	34
ECL	0.1 pM to 100 nM	31.6 fM	8
ECL	100 aM to 1 nM	62.1 aM	this work

Table 2. Recovery Tests for TB in Human Serum (n = 5)

sample	added	found	recovery (%)	RSD (%)
1	10 fM	9.69 fM	96.9	1.78
2	100 fM	101.92 fM	101.92	2.15
3	1 pM	0.98 pM	98	1.93
4	10 pM	9.75 pM	97.5	3.37
5	100 pM	103.58 pM	103.58	1.91

https://doi.org/10.1021/acs.analchem.1c05436
Anal. Chem. 2022, 94, 3685−3692

recoveries of target TB ranged from 96.9 to 103.58% with an RSD of 1.78−3.37%, which demonstrated that the TB sensor possessed prominent application potential in clinical analysis.

CONCLUSIONS

In this work, to improve the ECL signal and efficiency, the first conductive COF with a conductivity-enhanced ECL effect has been judiciously synthesized. The conductive HHTP-HATP-COF possessed excellent electrical conductivity and porous structures, which could speed up charge transport and improve the utilization ratio of ECL luminophores. As a result, the conductive HHTP-HATP-COF displayed higher ECL intensity and efficiency than low-conductive HHTP-DABZ-COF, HHTP, and HATP. More intriguingly, the ECL intensity of the HHTP-HATP-COF/$S_2O_8^{2-}$ system was further increased after pre-reduction electrolysis because of the accumulation of HHTP-HATP-COF$^{\bullet+}$. Based on the brilliant ECL performance of the HHTP-HATP-COF/$S_2O_8^{2-}$ system after pre-reduction electrolysis and the aptamer/protein proximity binding-induced 3D bipedal DNA walker amplification strategy, an "off−on" ECL sensor was designed and realized ultrasensitive determination of TB. In short, this work not only reported the first conductive COF with ECL sensing applications, which broadened the applied range of conductive COFs, but also provided effective strategies to enhance ECL emission, which shed new light on the design and synthesis of the high-performance COF-based ECL emitters.

ASSOCIATED CONTENT

Supporting Information

The Supporting Information is available free of charge at https://pubs.acs.org/doi/10.1021/acs.analchem.1c05436.

Materials and reagents; apparatus; experimental section; chemical structure of HHTP-HATP-COF and HHTP-DABZ-COF; PXRD patterns; infrared spectra of HHTP, HATP, and HHTP-HATP-COF; UV−vis absorption spectra of HHTP, HATP, and HHTP-HATP-COF; SEM of HHTP-HATP-COF; luminescence properties of HHTP-HATP-COF; rising ECL intensity of HHTP-HATP-COF; cathodic and anodic ECL transients of HHTP-HATP-COF; anodic ECL behaviors of the HHTP-HATP-COF; optimization of the ECL signal and experimental conditions of the ECL sensor; stable ECL intensities of the HHTP-HATP-COF/$S_2O_8^{2-}$ system before and after pre-reduction electrolysis; ECL, CV, and EIS characterizations of the ECL sensor; and the relative ECL efficiency calculation (PDF)

AUTHOR INFORMATION

Corresponding Author

Dong-Rong Xiao − *Key Laboratory of Luminescence Analysis and Molecular Sensing (Southwest University), Ministry of Education, College of Chemistry and Chemical Engineering, Southwest University, Chongqing 400715, PR China;* orcid.org/0000-0003-4610-1969; Phone: +86-23-68252360; Email: xiaodr98@swu.edu.cn; Fax: +86-23-68254000

Authors

Jin-Ling Zhang − *Key Laboratory of Luminescence Analysis and Molecular Sensing (Southwest University), Ministry of Education, College of Chemistry and Chemical Engineering, Southwest University, Chongqing 400715, PR China*

Li-Ying Yao − *Key Laboratory of Luminescence Analysis and Molecular Sensing (Southwest University), Ministry of Education, College of Chemistry and Chemical Engineering, Southwest University, Chongqing 400715, PR China*

Yang Yang − *Key Laboratory of Luminescence Analysis and Molecular Sensing (Southwest University), Ministry of Education, College of Chemistry and Chemical Engineering, Southwest University, Chongqing 400715, PR China*

Wen-Bin Liang − *Key Laboratory of Luminescence Analysis and Molecular Sensing (Southwest University), Ministry of Education, College of Chemistry and Chemical Engineering, Southwest University, Chongqing 400715, PR China;* orcid.org/0000-0002-9086-4974

Ruo Yuan − *Key Laboratory of Luminescence Analysis and Molecular Sensing (Southwest University), Ministry of Education, College of Chemistry and Chemical Engineering, Southwest University, Chongqing 400715, PR China;* orcid.org/0000-0003-3664-6236

Complete contact information is available at: https://pubs.acs.org/10.1021/acs.analchem.1c05436

Notes

The authors declare no competing financial interest.

ACKNOWLEDGMENTS

Thanks to the NSFC (21571149) and Innovation Support Program for Chongqing Overseas Returnees (cx2017007 and cx2018026).

REFERENCES

(1) Richter, M. M. *Chem. Rev.* **2004**, *104*, 3003−3036.
(2) Miao, W. *Chem. Rev.* **2008**, *108*, 2506−2553.
(3) Hu, L.; Xu, G. *Chem. Soc. Rev.* **2010**, *39*, 3275−3304.
(4) Han, Z. G.; Yang, Z. F.; Sun, H. S.; Xu, Y. L.; Ma, X. F.; Shan, D. L.; Chen, J.; Huo, S. H.; Zhang, Z.; Du, P. Y.; Lu, X. Q. *Angew. Chem., Int. Ed.* **2019**, *58*, 5915−5919.
(5) Zhao, Y.; Yu, J.; Xu, G.; Sojic, N.; Loget, G. *J. Am. Chem. Soc.* **2019**, *141*, 13013−13016.
(6) Huang, Y.; Lu, Y.; Huang, X.; Wang, J.; Qiu, B.; Luo, F.; Lin, Z. *Chem. Sci.* **2021**, *12*, 13151−13157.
(7) Zeng, W. J.; Wang, K.; Liang, W. B.; Chai, Y. Q.; Yuan, R.; Zhuo, Y. *Chem. Sci.* **2020**, *11*, 5410−5414.
(8) Wei, H.; Hu, G. B.; Liang, W. B.; Wang, J. M.; Lu, M. L.; Yuan, R.; Xiao, D. R. *Anal. Chem.* **2021**, *93*, 6239−6245.
(9) Zhang, Y.; Chai, Y.; Wang, H.; Yuan, R. *Anal. Chem.* **2019**, *91*, 14368−14374.
(10) Yao, L. Y.; Yang, F.; Hu, G. B.; Yang, Y.; Huang, W.; Liang, W. B.; Yuan, R.; Xiao, D. R. *Biosens. Bioelectron.* **2020**, *155*, 112099.
(11) Yang, Y.; Hu, G. B.; Liang, W. B.; Yao, L. Y.; Huang, W.; Yuan, R.; Xiao, D. R. *Nanoscale* **2019**, *11*, 10056−10063.
(12) Yang, Y.; Yao, L. Y.; Liang, W. B.; Huang, W.; Zhang, Y. J.; Zhang, J. L.; Yuan, R.; Xiao, D. R. *Chem. Commun.* **2021**, *57*, 4323−4326.
(13) Hu, G. B.; Xiong, C. Y.; Liang, W. B.; Yang, Y.; Yao, L. Y.; Huang, W.; Luo, W.; Yuan, R.; Xiao, D. R. *Biosens. Bioelectron.* **2019**, *135*, 95−101.
(14) Zhang, J. L.; Yang, Y.; Liang, W. B.; Yao, L. Y.; Yuan, R.; Xiao, D. R. *Anal. Chem.* **2021**, *93*, 3258−3265.
(15) Shi, X.; Ma, D.; Xu, F.; Zhang, Z.; Wang, Y. *Chem. Sci.* **2020**, *11*, 989−996.
(16) Li, H.; Chen, F.; Guan, X.; Li, J.; Li, C.; Tang, B.; Valtchev, V.; Yan, Y.; Qiu, S.; Fang, Q. *J. Am. Chem. Soc.* **2021**, *143*, 2654−2659.

(17) Gao, P.; Wang, M.; Chen, Y.; Pan, W.; Zhou, P.; Wan, X.; Li, N.; Tang, B. *Chem. Sci.* **2020**, *11*, 6882−6888.
(18) Li, Y. J.; Cui, W. R.; Jiang, Q. Q.; Wu, Q.; Liang, R. P.; Luo, Q. X.; Qiu, J. D. *Nat. Commun.* **2021**, *12*, 4735.
(19) Luo, R.; Lv, H.; Liao, Q.; Wang, N.; Yang, J.; Li, Y.; Xi, K.; Wu, X.; Ju, H.; Lei, J. *Nat. Commun.* **2021**, *12*, 6808.
(20) Li, S.; Ma, X.; Pang, C.; Wang, M.; Yin, G.; Xu, Z.; Li, J.; Luo, J. *Biosens. Bioelectron.* **2021**, *176*, 112944.
(21) Bian, G.; Yin, J.; Zhu, J. *Small* **2021**, *17*, 2006043.
(22) Guo, Z. C.; Shi, Z. Q.; Wang, X. Y.; Li, Z. F.; Li, G. *Coordin. Chem. Rev.* **2020**, *422*, 213465.
(23) Ding, X.; Guo, J.; Feng, X.; Honsho, Y.; Guo, J.; Seki, S.; Maitarad, P.; Saeki, A.; Nagase, S.; Jiang, D. *Angew. Chem., Int. Ed.* **2011**, *50*, 1289−1293.
(24) Zhu, H. J.; Lu, M.; Wang, Y. R.; Yao, S. J.; Zhang, M.; Kan, Y. H.; Liu, J.; Chen, Y. F.; Li, S. L.; Lan, Y. Q. *Nat. Commun.* **2020**, *11*, 497.
(25) Jin, S.; Sakurai, T.; Kowalczyk, T.; Dalapati, S.; Xu, F.; Wei, H.; Chen, X.; Gao, J.; Seki, S.; Irle, S.; Jiang, D. *Chem. − Eur. J.* **2014**, *20*, 14608−14613.
(26) Duhović, S.; Dincă, M. *Chem. Mater.* **2015**, *27*, 5487−5490.
(27) Yang, H.; Zhang, S.; Han, L.; Zhang, Z.; Xue, Z.; Gao, J.; Li, Y.; Huang, C.; Yi, Y.; Liu, H.; Li, Y. *ACS Appl. Mater. Interfaces* **2016**, *8*, 5366−5375.
(28) Wang, M. C.; Ballabio, M.; Wang, M.; Lin, H. H.; Biswal, B. P.; Han, X. C.; Paasch, S.; Brunner, E.; Liu, P.; Chen, M. W.; Bonn, M.; Heine, T.; Zhou, S. Q.; Canovas, E.; Dong, R. H.; Feng, X. L. *J. Am. Chem. Soc.* **2019**, *141*, 16810−16816.
(29) Song, X. Y.; Wang, X. Y.; Li, Y. S.; Zheng, C. Z.; Zhang, B. W.; Di, C. A.; Li, F.; Jin, C.; Mi, W. B.; Chen, L.; Hu, W. P. *Angew. Chem., Int. Ed.* **2020**, *59*, 1118−1123.
(30) Chen, T.; Dou, J. H.; Yang, L.; Sun, C.; Libretto, N. J.; Skorupskii, G.; Miller, J. T.; Dincă, M. *J. Am. Chem. Soc.* **2020**, *142*, 12367−12373.
(31) Li, W. H.; Deng, W. H.; Wang, G. E.; Xu, G. *EnergyChem.* **2020**, *2*, 100029.
(32) Peng, H.; Huang, Z.; Sheng, Y.; Zhang, X.; Deng, H.; Chen, W.; Liu, J. *Angew. Chem., Int. Ed.* **2019**, *58*, 11691−11694.
(33) Jin, Z.; Zhu, X.; Wang, N.; Li, Y.; Ju, H.; Lei, J. *Angew. Chem., Int. Ed.* **2020**, *59*, 10446−10450.
(34) Xu, Y.; Wang, Z.; Ding, C.; Luo, X. *Sens. Actuators B Chem.* **2020**, *322*, 128613.
(35) Deng, X.; Wu, S.; Li, Z.; Zhao, Y.; Duan, C. *Anal. Chem.* **2020**, *92*, 15908−15915.
(36) Gao, X.; Cai, Q.; Li, H.; Jie, G. *Anal. Chem.* **2020**, *92*, 6734−6740.
(37) Kong, L.; Wang, D.; Chai, Y.; Yuan, Y.; Yuan, R. *Anal. Chem.* **2019**, *91*, 10289−10294.
(38) Kou, Y.; Xu, Y.; Guo, Z.; Jiang, D. *Angew. Chem., Int. Ed.* **2011**, *50*, 8753−8757.
(39) Jhulki, S.; Kim, J.; Hwang, I. C.; Haider, G.; et al. *Chem* **2020**, *6*, 2035−2045.
(40) Marco, A. B.; Cortizo-Lacalle, D.; Perez-Miqueo, I.; Valenti, G.; Boni, A.; Plas, J.; Strutyński, K.; Feyter, S. D.; Paolucci, F.; Montes, M.; Khlobystov, A. N.; Melle-Franco, M.; Mateo-Alonso, A. *Angew. Chem., Int. Ed.* **2017**, *56*, 6946−6951.
(41) Tan, X.; Zhang, B.; Zou, G. *J. Am. Chem. Soc.* **2017**, *139*, 8772−8776.
(42) Ding, Z.; Quinn, B. M.; Haram, S. K.; Pell, L. E.; Korgel, B. A.; Bard, A. J. *Science* **2002**, *296*, 1293−1297.
(43) Zhang, X.; Zhang, B.; Miao, W.; Zou, G. *Anal. Chem.* **2016**, *88*, 5482−5488.
(44) Zhang, X.; Tan, X.; Zhang, B.; Miao, W.; Zou, G. *Anal. Chem.* **2016**, *88*, 6947−6953.

Recommended by ACS

Construction of sp² Carbon-Conjugated Covalent Organic Frameworks for Framework-Induced Electrochemiluminescence
Qiu-Xia Luo, Jian-Ding Qiu, *et al.*
SEPTEMBER 21, 2021
ACS APPLIED ELECTRONIC MATERIALS
READ

2D Conductive Covalent Organic Frameworks with Abundant Carbonyl Groups for Electrochemical Sensing
Kai Niu, Xianbo Lu, *et al.*
OCTOBER 20, 2022
ACS SENSORS
READ

Nanoscale Covalent Organic Frameworks with Donor–Acceptor Structures as Highly Efficient Light-Responsive Oxidase-like Mimics for Colorimetric Detectio...
Guorong Li, Zian Lin, *et al.*
OCTOBER 12, 2021
ACS APPLIED MATERIALS & INTERFACES
READ

Construction and Sensing Amplification of Raspberry-Shaped MOF@MOF
Ming-Xue Wu, Xiaomin Liu, *et al.*
MARCH 10, 2022
INORGANIC CHEMISTRY
READ

Get More Suggestions >

https://doi.org/10.1021/acs.analchem.1c05436
Anal. Chem. 2022, 94, 3685−3692